



Article

# Structural and Fluorine Plasma Etching Behavior of Sputter-Deposition Yttrium Fluoride Film

Wei-Kai Wang \*, Yu-Xiu Lin and Yi-Jie Xu

Department of Materials Science and Engineering, Da-Yeh University, Changhua 51591, Taiwan; h63290@gmail.com (Y.-X.L.); pa821221@yahoo.com.tw (Y.-J.X.)

\* Correspondence: wk@mail.dyu.edu.tw; Tel.: +886-5-8511-888 (ext. 2606); Fax: +886-5-8511-666

Received: 28 October 2018; Accepted: 10 November 2018; Published: 14 November 2018



**Abstract:** Yttrium fluoride ( $\text{YF}_3$ ) films were grown on sapphire substrate by a radio frequency magnetron using a commercial ceramic target in a vacuum chamber. The structure, composition, and plasma etching behavior of the films were systematically investigated. The  $\text{YF}_3$  film was deposited at a working pressure of 5 mTorr and an RF power of 150 W. The substrate-heating temperature was increased from 400 to 700 °C in increments of 100 °C. High-resolution transmission electron microscopy (HRTEM) and X-ray diffraction results confirmed an orthorhombic  $\text{YF}_3$  structure was obtained at a substrate temperature of 700 °C for 2 h. X-ray photoelectron spectroscopy revealed a strongly fluorinated bond (Y–F bond) on the etched surface of the  $\text{YF}_3$  films. HRTEM analysis also revealed that the  $\text{YF}_3$  films became yttrium-oxyfluorinated after exposure to fluorocarbon plasma. The etching depth was three times lower on  $\text{YF}_3$  film than on  $\text{Al}_2\text{O}_3$  plate. These results showed that the  $\text{YF}_3$  films have excellent erosion resistance properties compared to  $\text{Al}_2\text{O}_3$  plates.

**Keywords:** yttrium fluoride; films; plasma processing equipment

## 1. Introduction

Silicon-oxide series of ceramics, such as  $\text{SiO}_2$  and  $\text{Al}_2\text{O}_3$  coatings, are valued for their hardness, high wear resistance, dielectric strength, high corrosion resistance, and chemical stability. They have been extensively used as plasma-resistant materials in plasma etching equipment and in the deposition thin-film processing semiconductor industry [1,2]. They are also popular shield materials that protect the interior ceramic parts, chamber windows, cover baffles, rings, and reactor chamber walls of plasma equipment from corrosive fluorocarbon gases (e.g.,  $\text{C}_2\text{F}_6$ ,  $\text{CF}_4$ ,  $\text{CHF}_3$ , and  $\text{C}_2\text{F}_6$ ) [3]. However, on the inner walls of the processing chamber, these oxide materials easily interact with fluorine-based plasma, causing significant erosion and particle generation [4]. As integrated circuits continue to downscale to the nanoscopic level, particle contaminants in their wafers are becoming increasingly worrisome, because they short-current the integration circuit and reduce mass-production yield [5]. Yttrium oxide ( $\text{Y}_2\text{O}_3$ ) promises to replace  $\text{SiO}_2$  and  $\text{Al}_2\text{O}_3$  as the material of plasma-facing inner walls, owing to its much higher chemical stability and reduced erosion rate [6]. Nevertheless, as pointed out by mass-production factories,  $\text{Y}_2\text{O}_3$  inner wall coatings contain pores and crack defects that release particles into the plasma by flake-off [7]. Yttrium fluoride ( $\text{YF}_3$ ) coatings have recently attracted substantial attention because their high plasma erosion resistance prevents the generation of fluoride particles on the chamber wall surface, reducing particulate contamination [8]. Moreover,  $\text{YF}_3$  reportedly has a high dielectric strength [9]. Thus,  $\text{YF}_3$  coating is a new plasma-facing material. Researchers have fabricated protective coatings in chamber walls using a plasma spray technique. However, as the spray method rapidly forms thick films with porous structures and rough surfaces, it might introduce critical particle impurities during the semiconductor plasma deposition/etching process [10]. Vacuum coating techniques such as magnetron sputtering can address these problems.

To our knowledge, sputtered YF<sub>3</sub> films and their erosion behavior under fluorocarbon plasma etching had not previously been investigated. Herein, we investigate the composition, structure, erosion behavior, and surface morphology changes of YF<sub>3</sub> films on sapphire substrate, prepared by magnetron sputtering.

## 2. Materials and Methods

The sputter material was YF<sub>3</sub> ceramic target (99.99% purity, 2 inch diameter, 3 mm thickness). YF<sub>3</sub> thin films were deposited on c-plane sapphire substrate (single crystal of Al<sub>2</sub>O<sub>3</sub>) at room temperature by radio frequency magnetron sputtering in a vacuum chamber. The substrates were cleaned before deposition, first in acetone and alcohol, and then by ultrasonic cleansing in de-ionized (DI) water for 30 min. They were blow-dried in nitrogen gas. The sputtering gas was high-purity argon (99.995%), maintained at a constant flow rate (~100 sccm). The sputtering process was performed under a base chamber pressure of approximately  $1.5 \times 10^{-5}$  torr, with turbo molecular and oil diffusion pumps. The plasma generation was activated by RF power at 13.56 MHz. The target–substrate distance was 15 cm. To ensure uniform film thickness, the substrate holder was rotated at 20 rpm during the deposition process. Substrate heating temperature was varied from 400 to 700 °C in steps of 100 °C. The sputter deposition conditions of the YF<sub>3</sub> films are detailed in Table 1. The plasma etching behaviors of all samples were performed using an inductively-coupled plasma etcher. The etching gases mixed were CF<sub>4</sub> and O<sub>2</sub>. The etching conditions are shown in Table 2.

**Table 1.** Experimental parameters of sputter deposition conditions of YF<sub>3</sub> film.

Parameters	Conditions
RF power (W)	150
Duration (hours)	2
Substrate temperature (°C)	400–700
Substrate rotation (rpm)	20
Working pressure (mTorr)	5
Substrate to target distance (cm)	15
Argon gas flow rate (sccm)	100

**Table 2.** Plasma etching conditions.

Parameters	Condition
RF power (W)	800
RF power, bias (W)	100
Pressure (mTorr)	3
CF <sub>4</sub> (sccm)	25
O <sub>2</sub> (sccm)	5
Etching time (min)	10, 20, 30

The surface morphology, microstructure, and elemental analysis of these coating samples were analyzed by scanning electron microscopy (SEM, S-3000H, Hitachi, Tokyo, Japan) coupled with energy dispersive X-ray diffraction (EDX), atomic force microscopy (AFM, DI-3100, Veeco, New York, NY, USA), and high-resolution transmission electron microscopy (HRTEM, H-600, Hitachi, Tokyo, Japan). The sample compositions were examined by X-ray photoelectron spectroscopy (XPS, PHI 5000 VersaProbe, ULVAC-PHI, Kanagawa, Japan) using a monochromatic Cu K $\alpha$  X-ray source ( $\lambda = 1.541874$  Å) at a passing energy of 20 eV with a spot size of 650  $\mu$ m. After XPS, the sample surface was etched using focused argon-ion sputtering to investigate the chemical compositional depth profile (Thermo Scientific K-Alpha). Finally, the photoelectron spectrum resulting from the core energy levels of yttrium 3D states was deconvoluted by a fitting software program (Thermo Fisher Scientific, Inc., Waltham, MA, USA) to estimate the contributions from bonding with fluorine elements.

### 3. Results and Discussion

Figure 1 depicts the XRD scan patterns of  $\text{YF}_3$  films deposited on  $\text{Al}_2\text{O}_3$  substrate at 400, 500, 600, and 700 °C. All  $\text{YF}_3$  samples were polycrystalline, and their structural orientations depended on the substrate temperature in the deposition process. The (020) plane of the orthorhombic  $\text{YF}_3$  phase was formed at substrate temperatures above 500 °C, which is in agreement with the reported data (JCPDS card files No. 74-0911) [11]. Moreover, the preferential orientation of the orthorhombic  $\text{YF}_3$  crystal structure differed in films fabricated at different temperatures. This might be attributed to the high kinetic energy imparted to  $\text{YF}_3$  molecules at high substrate temperatures, which enables them to migrate and rearrange on the substrate surface.  $\text{YF}_3$  samples fabricated at higher temperatures also showed a weak peak of the cubic  $\text{Y}_2\text{O}_3$  phase (400) plane (JCPDS card files No. 79-1716), indicating contamination by oxygen atoms during the sputtering process [9]. As substrate temperature increases,  $\text{Y}_2\text{O}_3$  formation might be favored by the higher instability of fluoride in the  $\text{YF}_3$  crystal lattice. Unstable F ions in the lattice can be gradually replaced by environmental oxygen atoms. Therefore, the number of oxygen atoms in the crystal lattice increases with increasing temperature, forming  $\text{Y}_2\text{O}_3$  (see Figure 1). When  $\text{YF}_3$  film was deposited at a lower substrate temperature, an amorphous structure was formed. Amorphous film usually has a loose structure, resulting in greater thickness and a higher growth rate. In contrast, with increasing substrate temperature, the  $\text{YF}_3$  film became crystalline, and its crystal was relatively ordered. This indicates that a denser structure was found in the  $\text{YF}_3$  film grown at higher substrate temperatures, leading to its smaller thickness and lower growth rate. In TEM analysis, the  $\text{YF}_3$  films exhibited nanocrystalline grains with an average size of 5–20 nm (Figure 2). The regular ring-like electron diffraction pattern of a selected area (Figure 2, inset) implies a polycrystalline structure of  $\text{YF}_3$  film, consistent with the XRD result.

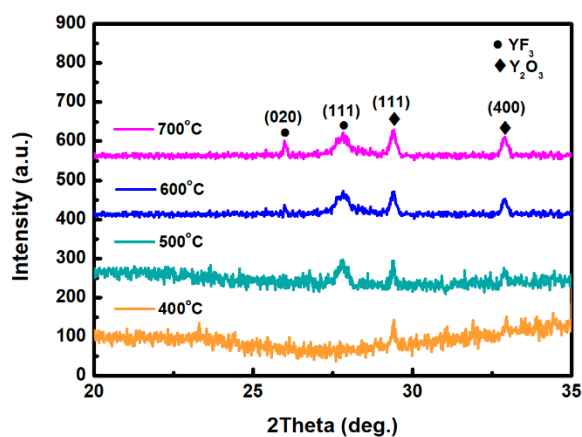


**Figure 1.** XRD patterns of the as-deposited yttrium fluoride ( $\text{YF}_3$ ) films grown at 400, 500, 600, and 700 °C.

Figure 3a,b show the XPS survey spectra in the 0–1200 eV range of the  $\text{YF}_3$  films before and after  $\text{CF}_4/\text{O}_2$  plasma etching, respectively. To collect the atomic signals, all samples were bombarded by argon ions for 2 min. The XPS peaks in the as-grown  $\text{YF}_3$  thin film (Figure 3a) correspond to Y, F, O, and C elements. The Y and F elements existed in the original  $\text{YF}_3$  film, and an O1s peak arose from oxygen contamination during the sputter deposition process. This result is consistent with previous reports [12]. After exposure to  $\text{CF}_4/\text{O}_2$  plasma, the spectrum of the  $\text{YF}_3$  film exhibited an enhanced F1s peak and an additional C1s peak. The former feature is attributed to the high fluorine content of  $\text{YF}_3$ , and the latter indicates the formation of a carbon-polymer surface layer under fluorocarbon plasma etching (Figure 3b). Figure 4a,b plot the compositions of the  $\text{YF}_3$  films as functions of sputtering time before and after exposure to the  $\text{CF}_4/\text{O}_2$  plasma, respectively. Before exposure to the plasma, the maximum F content was 37% and the minimum O content was 32% (Figure 4a). This result indicates a two-phase mixture of  $\text{YF}_3$  and  $\text{Y}_2\text{O}_3$  in the film, consistent with a previous study that reported a

deficiency of fluorine atoms during the sputter deposition process [13]. The maximum percentage of F atoms in the etched sample was 44.69%, implying a fluorination layer on the  $\text{YF}_3$  specimen (Figure 4b). Similar results were observed in a previous study of surface fluorination by  $\text{CF}_4/\text{O}_2$  plasma etching [14]. The carbon content on the  $\text{YF}_3$  surface decreased abruptly with sputtering time, indicating a very thin carbon polymer layer on the etched surface. This is because of interactions between the fluorocarbon plasma and Si-based materials, which generate carbon polymer and a  $\text{SiF}_x\text{O}_y$  reaction layer [15].

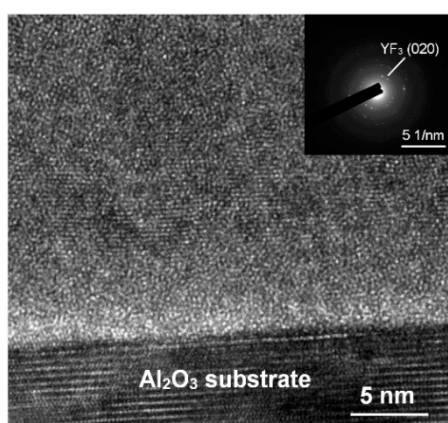


Figure 2. TEM microstructure and selected area diffraction (inset) of  $\text{YF}_3$  film.

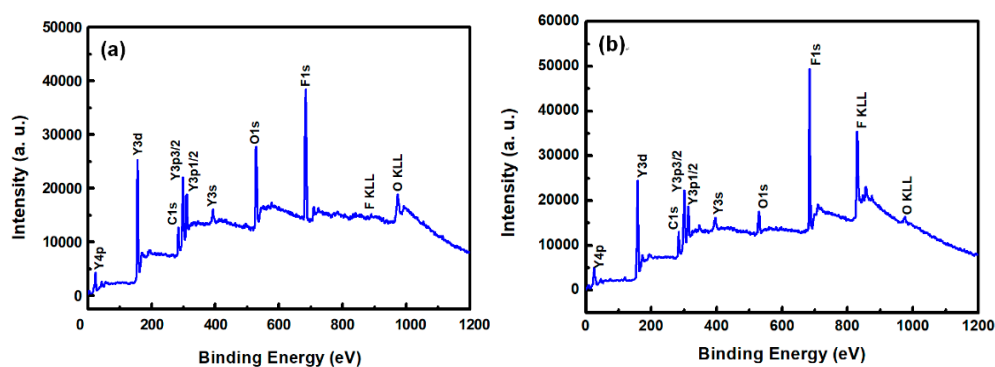


Figure 3. XPS survey spectra of the surfaces of the  $\text{YF}_3$  thin films (a) before and (b) after exposure to  $\text{CF}_4/\text{O}_2$  plasma (under bombardment with argon ions for two minutes).

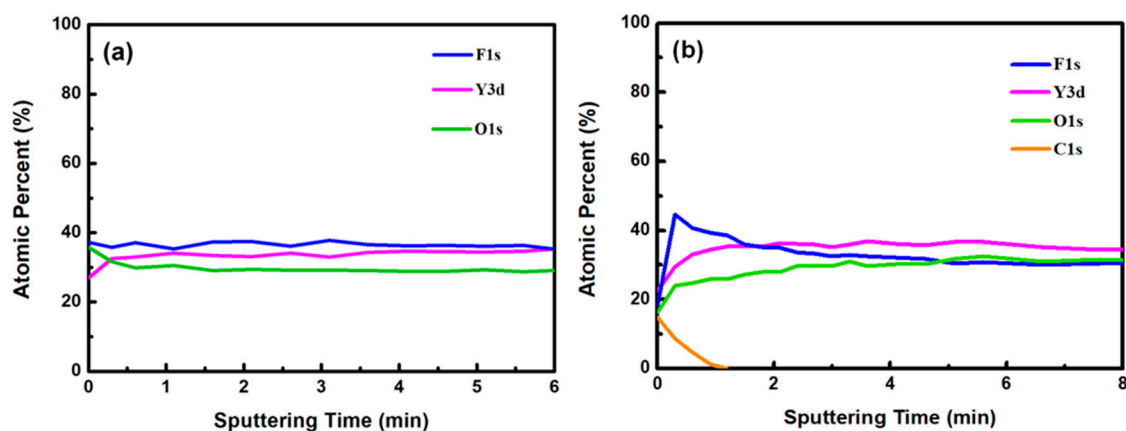
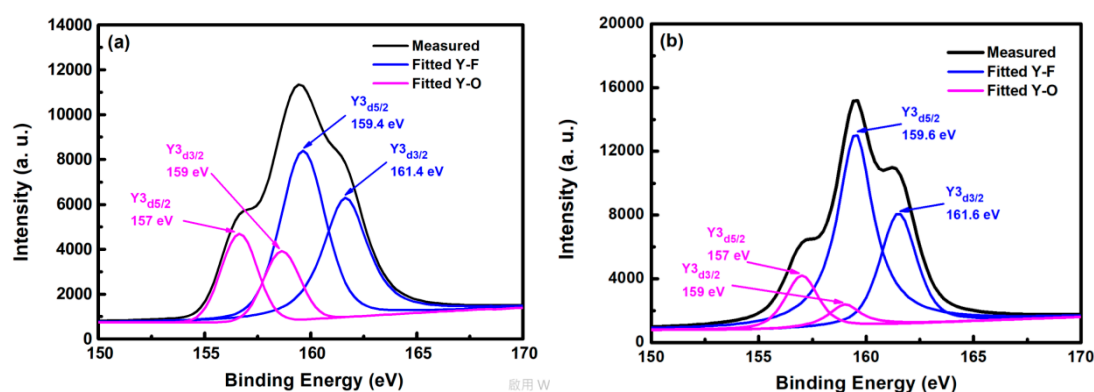


Figure 4. Atomic percentages of  $\text{YF}_3$  film versus sputtering time (a) before and (b) after surface exposure to  $\text{CF}_4/\text{O}_2$  plasma.

Figure 5 shows the XPS spectra of yttrium atoms of the  $\text{YF}_3$  film after  $\text{CF}_4/\text{O}_2$  plasma etching. In the curve-fitted XPS spectra of the  $\text{YF}_3$  film, two peaks represent two bonding sources for Y cations, that is, the Y3d peak splits into a doublet ( $\text{Y}3d_{5/2}$  and  $\text{Y}3d_{3/2}$  electrons) with a binding-energy separation of 2 eV. The two yttrium bonding sources are consistent with the XPS standard [16]. The  $\text{Y}3d_{5/2}$  and  $\text{Y}3d_{3/2}$  peaks in the spectrum of the as-deposited  $\text{YF}_3$  film (Figure 5a) deconvolute into four peaks. The two peaks located at higher binding energies (159.4 and 161.4 eV) correspond to Y–F bonding in the  $\text{YF}_3$  film, whereas those at lower binding energies (157 and 159 eV) are ascribed to Y–O bonding. In the XPS spectra of etched  $\text{YF}_3$  film surface, the peaks are more intense than in the un-etched specimen (Figure 5b). Again, the strong doublet at higher binding energies (159.6 and 161.6 eV) and the weak doublet at lower binding energies (157 and 159 eV) correspond to Y–F and Y–O bonding, respectively. The higher XPS binding energy of the Y–F bonding can be attributed to the higher electronegativity of fluorine atoms (4.0) than oxygen atoms (3.5) [17]. Consequently, more electrons are transferred to fluorine, decreasing the electron density around the cation and enhancing the binding energy. Meanwhile, the intensity ratio of Y–F to Y–O bonds was estimated as 2.1 on etched  $\text{YF}_3$  films, indicating strong chemical interaction between the  $\text{YF}_3$  films and the fluorocarbon plasma.



**Figure 5.** X-ray photoelectron spectra of  $\text{YF}_3$  film (a) before and (b) after exposure to fluorocarbon plasma.

To evaluate the plasma erosion resistance of as-deposited  $\text{YF}_3$  films, the etching rate of the  $\text{YF}_3$ -coated  $\text{Al}_2\text{O}_3$  substrate was measured after exposure to the  $\text{CF}_4/\text{O}_2$  plasma for different etching times. The etching rate of bare  $\text{Al}_2\text{O}_3$  crystal was used as the reference. Figure 6 shows that the etching depths of both samples linearly increased with increasing etching time. After 30 min, the etching depth reached 120  $\mu\text{m}$  in the sapphire, but only 38  $\mu\text{m}$  in  $\text{YF}_3$ . The erosion resistance of the  $\text{YF}_3$  film to  $\text{CF}_4/\text{O}_2$  plasma etching was more than three times higher than that of sapphire crystal. This is attributed to the chemical stability of  $\text{YF}_3$  in a chemical environment dominated by fluorocarbon plasma. The surface morphologies and roughness of the  $\text{YF}_3$  films etched for different lengths of time were measured by AFM measurements, with a scanning area of  $5 \mu\text{m}^2$ . The surface roughness results are shown in Figure 7. The etching time of the  $\text{CF}_4/\text{O}_2$  plasma did not remarkably influence the surface roughness of the  $\text{YF}_3$  film.

Figure 8a,b show the surface microstructures of  $\text{YF}_3$  and  $\text{Al}_2\text{O}_3$  samples, respectively, after the etching experiment. The micrographs were acquired by optical microscopy (OM). The right and left images in each panel show the un-etched and etched surfaces, respectively. The step height of the  $\text{Al}_2\text{O}_3$  sample changed after  $\text{CF}_4/\text{O}_2$  plasma etching. These images confirm the hardness and stronger  $\text{CF}_4/\text{O}_2$  corrosion resistance of the  $\text{YF}_3$  films compared to conventional  $\text{Al}_2\text{O}_3$  substrate.

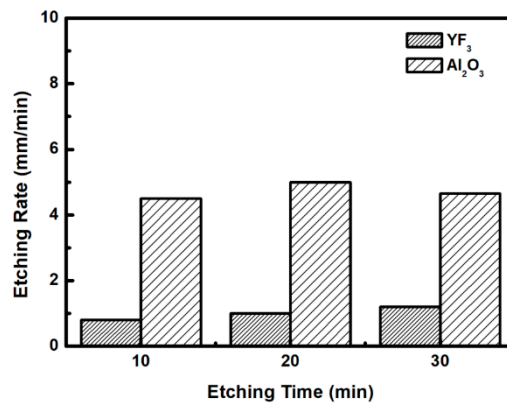


**Figure 6.** Etching depths of the YF<sub>3</sub> film and Al<sub>2</sub>O<sub>3</sub> substrates after different CF<sub>4</sub>/O<sub>2</sub> plasma exposure times.

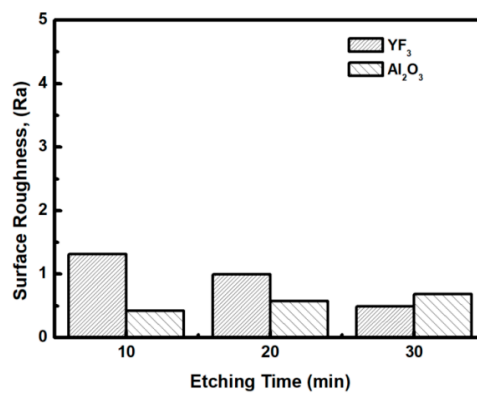


**Figure 7.** Surface roughness of YF<sub>3</sub> and Al<sub>2</sub>O<sub>3</sub> exposed to fluorocarbon plasma for different etching times.

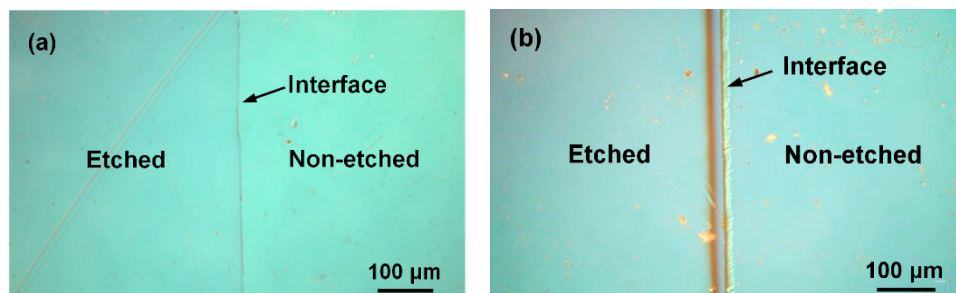


**Figure 8.** Optical micrographs of the (a) YF<sub>3</sub> and (b) Al<sub>2</sub>O<sub>3</sub> substrates after exposure to fluorocarbon plasma.

AlF<sub>3</sub> is a typical fluoride of Al<sub>2</sub>O<sub>3</sub> materials [4]. The boiling temperature of YF<sub>3</sub> (2230 °C) is higher than the sublimation temperature of AlF<sub>3</sub> (1275 °C). Hence, YF<sub>3</sub> is more stable and more difficult to vaporize than AlF<sub>3</sub>. Therefore, its fluorinated layer can be removed by a physical sputtering process. The sputtering yields of the films are inversely proportional to sublimation enthalpies of their compounds [18]. The sublimation enthalpy of YF<sub>3</sub> ( $481 \pm 21$  kJ/mol) is higher than that of AlF<sub>3</sub> ( $301 \pm 4$  kJ/mol). Moreover, the enthalpy of formation of the metal–oxygen bond is lower in YF<sub>3</sub> ( $-392$  kJ mol<sup>-1</sup>) than in Al<sub>2</sub>O<sub>3</sub> ( $-279$  kJ mol<sup>-1</sup>). Therefore, YF<sub>3</sub> is chemically more stable than Al<sub>2</sub>O<sub>3</sub> [19]. In particular, YF<sub>3</sub> is extremely stable under the fluorocarbon plasma etching process.

Figure 9 shows a cross-sectional HRTEM image of the YF<sub>3</sub> film after CF<sub>4</sub>/O<sub>2</sub> plasma exposure. Continuous and nearly-complete lattice fringes were observed near the surface, indicating that the YF<sub>3</sub> ceramic crystalline lattice was not distorted by the fluorine plasma irradiation. Furthermore,

the d-spacings of the near surface of film were 3.131 Å (blue dotted circle) and 2.621 Å (red dotted circle), very close to the d-spacings of the altered layers of yttrium oxyfluoride (YOF): 3.147 Å (006) and 2.698 Å (104) [11]. The thin YOF layer formed on the YF<sub>3</sub> surface plays a protective role, suppressing the particle generation during CF<sub>4</sub>/O<sub>2</sub> plasma etching process. The reaction and formation of an altered YOF layer has been reported previously [14]. Therefore, YF<sub>3</sub> film is a very attractive plasma-corrosion-resistant material that produces fewer contamination particles during the semiconductor fabrication process.

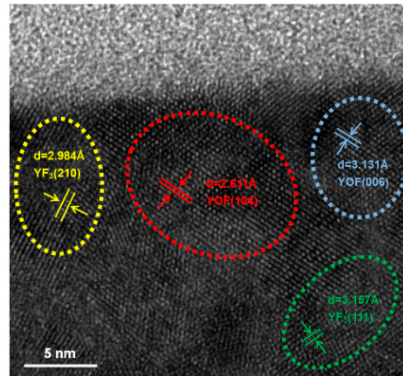


**Figure 9.** Cross-sectional high-resolution transmission electron microscopy (HRTEM) image of the YF<sub>3</sub> film after exposure to fluorine plasma.

#### 4. Conclusions

YF<sub>3</sub> films were successfully deposited through radio frequency magnetron sputtering on sapphire substrates at different temperatures. HRTEM and XRD results revealed polycrystalline YF<sub>3</sub> films with an orthorhombic structure. XPS results confirmed the superior chemical stability of YF<sub>3</sub> film after fluorocarbon plasma treatment. The robustness of YF<sub>3</sub> film was confirmed to be more than that of Al<sub>2</sub>O<sub>3</sub> film after the plasma exposure. The YF<sub>3</sub> film is expected to provide a more protective barrier than Al<sub>2</sub>O<sub>3</sub> or quartz plates in the fluorine plasma etching process.

**Author Contributions:** Conceptualization: W.-K.W.; Methodology: Y.-X.L., Y.-J.S. and W.-K.W.; Data curation: Y.-X.L., Y.-J.S. and W.-K.W.; Writing—original draft preparation: Y.-X.L., Y.-J.S. and W.-K.W.; Writing—review and editing: W.-K.W.

**Funding:** This research was funded by the Ministry of Science and Technology of Taiwan (No. 107-2221-E-212-004).

**Acknowledgments:** The authors wish to express their sincere gratitude for the technical support from the Advanced Industry Technology Centre of National Chung Hsing University, Taiwan.

**Conflicts of Interest:** The authors declare no conflict of interest.

#### References

- Kim, D.M.; Kim, K.B.; Yoon, S.Y.; Oh, S.Y.; Kim, H.T.; Lee, S.M. Effects of artificial pores and purity on the erosion behaviors of polycrystalline Al<sub>2</sub>O<sub>3</sub> ceramics under fluorine plasma. *J. Ceram. Soc.* **2009**, *117*, 863–867. [CrossRef]
- Zavareh, M.A.; Sarhen, A.A.D.M.; Razak, B.B.; Basirun, W.J. Plasma thermal spray of ceramic oxide coating on carbon steel with enhanced wear and corrosion resistance for oil and gas applications. *Ceram. Int.* **2014**, *40*, 14267–14277. [CrossRef]
- Fukumoto, H.; Fujikake, I.; Takao, Y.; Eriguchi, K.; Ono, K. Plasma chemical behavior of reactants and reaction products during inductively coupled CF<sub>4</sub> plasma etching of SiO<sub>2</sub>. *Plasma Sources Sci. Technol.* **2009**, *18*, 045027. [CrossRef]
- Kitamura, T.; Mizuno, H.; Kato, N.; Aoki, I. Plasma-erosion properties of ceramic coating prepared by plasma spraying. *Mater. Trans.* **2006**, *47*, 1677–1683. [CrossRef]
- Duc, L.M.; Tan, C.M.; Luo, M.; Leng, I.C.H. Maintenance scheduling of plasma etching chamber in wafer fabrication for high-yield etching process. *IEEE Trans. Semicond. Manuf.* **2014**, *27*, 204–211. [CrossRef]

6. Iwasawa, J.; Nishimizu, R.; Tokita, M.; Kiyohara, M.; Uematsu, K. Plasma-resistant dense yttrium oxide film prepared by aerosol deposition process. *J. Am. Ceram. Soc.* **2007**, *90*, 2327–2332. [[CrossRef](#)]
7. Mun, S.Y.; Shin, K.C.; Lee, S.S.; Kwak, J.S.; Jeong, J.Y.; Jeong, Y.H. Etch defect reduction using SF<sub>6</sub>/O<sub>2</sub> plasma cleaning and optimizing etching recipe in photo resist masked gate poly silicon etch process. *Jpn. J. Appl. Phys.* **2005**, *44*, 4891–4895. [[CrossRef](#)]
8. Kim, D.M.; Oh, Y.S.; Kim, S.; Kim, H.T.; Lim, D.S.; Lee, S.M. The erosion behaviors of Y<sub>2</sub>O<sub>3</sub> and YF<sub>3</sub> coatings under fluorocarbon plasma. *Thin Solid Films* **2011**, *519*, 6698–6702. [[CrossRef](#)]
9. Lin, T.K.; Wu, D.S.; Huang, S.Y.; Wang, W.K. Characteristics of yttrium fluoride and yttrium oxide coatings for plasma process equipment prepared by atmospheric plasma spraying. *Jpn. J. Appl. Phys.* **2016**, *55*, 126201. [[CrossRef](#)]
10. Chakravarthy, Y.; Bhandari, S.; Chaturvedi, V.; Pragatheeswaran, A.; Nagraj, A.; Thiyagarajan, T.K.; Ananthapadmanaban, P.V.; Das, A.K. Plasma spray deposition of yttrium oxide on graphite, coating characterization and interaction with molten uranium. *J. Eur. Ceram. Soc.* **2015**, *35*, 781–794. [[CrossRef](#)]
11. Chai, G.D.; Dong, G.P.; Qiu, J.R.; Zhang, Q.Y.; Yang, Z.M. Phase transformation and intense 2.7 mm emission from Er<sup>3+</sup> doped YF<sub>3</sub>/YOF submicron-crystals. *Sci. Rep.* **2013**, *3*, 1598. [[CrossRef](#)] [[PubMed](#)]
12. Pei, L.; Jiapi, Z.; Yuankun, Z.; Jiecai, H. Preparation and optical properties of sputtered-deposition yttrium fluoride film. *Nucl. Instrum. Methods Phys. Res. Sect. B* **2013**, *307*, 429–433. [[CrossRef](#)]
13. Quesnel, E.; Berger, M.; Duca, D.; Pelle, C.; Pierre, F. Near-UV to IR optical characterization of YF<sub>3</sub> thin films deposited by evaporation and ion beam processes. *Proc. SPIE* **1996**, *2776*, 366–372.
14. Lin, T.K.; Wang, W.K.; Huang, S.Y.; Tasi, C.T.; Wu, D.S. Comparison of erosion behavior and particle contamination in mass-production CF<sub>4</sub>/O<sub>2</sub> plasma chambers using Y<sub>2</sub>O<sub>3</sub> and YF<sub>3</sub> protective coatings. *Nanomaterials* **2017**, *7*, 183. [[CrossRef](#)] [[PubMed](#)]
15. Matsui, M.; Tatsumi, T.; Sekine, M. Observation of surface reaction layers formed in highly selective SiO<sub>2</sub> etching. *J. Vac. Sci. Technol.* **2001**, *19*, 1282–1888. [[CrossRef](#)]
16. Moulder, J.F.; Stickle, W.F.; Sobol, P.E.; Bomben, K.D. *Handbook of X-ray Photoelectron Spectroscopy*; Physical Electronics: Eden Prairie, MN, USA, 1995; p. 10.
17. Zhong, H.X.; Hong, J.M.; Cao, X.F.; Chen, X.T.; Xue, Z.L. Ionic-liquid-assisted synthesis of YF<sub>3</sub> with different crystalline phases and morphologies. *Mater. Res. Bull.* **2009**, *44*, 623–628. [[CrossRef](#)]
18. Cao, Y.C.; Zhao, L.; Luo, J.; Wang, K.; Zhang, B.P.; Yokota, H.; Ito, Y.; Li, J.F. Plasma etching behavior of Y<sub>2</sub>O<sub>3</sub> ceramics: Comparative study with Al<sub>2</sub>O<sub>3</sub>. *Appl. Surf. Sci.* **2016**, *366*, 304–309. [[CrossRef](#)]
19. Brunetti, B.; Piacente, V.; Scardala, P. Torsion vapor pressure and sublimation enthalpies of aluminum trifluoride and aluminum trichloride. *J. Chem. Eng. Data* **2009**, *54*, 940–944. [[CrossRef](#)]

